Proceedings of ICFDP7
Seventh International Congress On Fluid Dynamics & Propulsion
December 18-20, 2001, Cairo, Egypt

ICFDP7-2001016

EFFECT OF GROOVES GEOMETRY ON CHARCTERISTICS OF STRONG ADVERSE PRESSURE GRADIENT FLOW

Maher G. Higazy
Faculty of Engineering,
Shoubra, Zagazig University,
Cairo, Egypt

Nazih N. Bayomi
Faculty of Engineering,
Mataria, Helwan University,
Cairo, Egypt

ABSTRACT

Experimental investigation was carried out in order to determine the effect of grooves geometry configuration on separated boundary layer. The grooves were situated in a strong adverse pressure gradient flow. Ten rectangular and skewed grooves were used to investigate the effect on the separated boundary layer similar to wall-stall effect in compressors. The measurements were carried out on a two dimensional groove in a low speed wind tunnel. The wind tunnel has specially designed adjustable roof to accommodate the strong adverse pressure gradient required for the investigation.

The time average pressure coefficient of the grooves was measured and the boundary layer integral characteristics were obtained behind the ten different groove goemetries. The grooves presence were causing a an alteration in the skin friction of the boundary layers i.e. elimination or reducing the high-pressure area near the downstream of the grooves. Different types of grooved shaped generates lower pressure areas that would reduce the wall stall phenomena. Skewed grooves were reducing the boundary layer shape factor and reducing the skin friction of the surface enhanced than rectangular grooves.

NOTATION

c_f skin friction coefficient using the law of the wall,
Cp pressure coefficient, $Cp= (p_{(y)}-p_{st})/q_\infty=(p_{(y)}-p_{st})/(p_{t\infty}-p_{st\infty})$
D groove depth, mm,
G defect shape factor,
H boundary layer shape factor,
L length of working section from trip edge,
l groove length, mm,
M Mach number,
$p_{(y)}$ measured surface static pressure,
p_{st} measured static pressure on groove walls and floor,
$p_{t,\infty}$ free-stream total pressure,
q_∞ free-stream dynamic pressure,
U local freestream velocity, m/sec,
U^+ law of the wall coordinate, u/u_τ
U_∞ freestream velocity, m/sec.,
u local velocity profile, m/sec,
u_τ local skin friction velocity, m/sec, $U(0.5\ c_f)^{0.5}$
x distance in streamwise direction,
Y^+ law of the wall coordinate, yu_τ/ν,
y normal distance from the wall,
z distance normal to the flat plate,
β pressure gradient parameter,
δ boundary layer thickness, mm.,
δ* boundary layer displacement thickness,
ν kinematic viscosity,
θ boundary layer momentum thickness,
ρ fluid density,
τ_w wall shear stress,

Subscript
b back face,
i inclined face,
f front face,

INTRODUCTION

In axial compressors, rotating stall is a flow phenomenon, which has been the subject of many detailed experimental and theoretical investigations. An early survey of the subject was given by Emmons et al. [1]. The occurrence of stall phenomena in axial compressors is of major concern to both manufactures and users. In addition, the extension of the operating range towards lower mass flow rates is desired in many compression systems characterized by variable operating conditions. Therefore, it has been recognized for some time that the presence of a grooved or perforated casing over the tips of an axial compressor rotor can be extremely beneficial in extending the stall margin of the machine. Many investigations of different types of casing

configurations have been carried out under widely varying flow conditions and have demonstrated that the range of usefulness of these casing configurations extends from compressor operation in basically incompressible flow (M_{TIP}≈0.10) to the supersonic flow regime (M_{TIP}≈1.5). Greitzer et al. [2] observed that there are two types of stall, which could be found in a compressor blade row, namely, "blade stall" or "wall stall". Blade stall is, roughly speaking, a two-dimensional type of stall where a significant part of the blade has a large wake leaving the blade suction surface. Wall stall connected with the boundary layer on the outer casing. Figure (1) illustrates the two types of stall**.** Greitzer et al. [2], also, found that the response to casing treatment depended conspicuously upon the type of stall encountered. As predicted from their design study, the high solidity blading ($\sigma = 2$) resulted in the production of a wall stall, while the flow solidity ($\sigma=1$) blading gave a blade stall.

According to Haupt et al. [3]**,** on the edge of rotating stall, reverse flow appears from the outlet of the rotor along the casing toward the inlet in axial compressors. Then, the reverse flow appears to be common feature for the occurrence of rotating stall, independently of the type of turbo-compressors, Johnson and Greitzer [4].

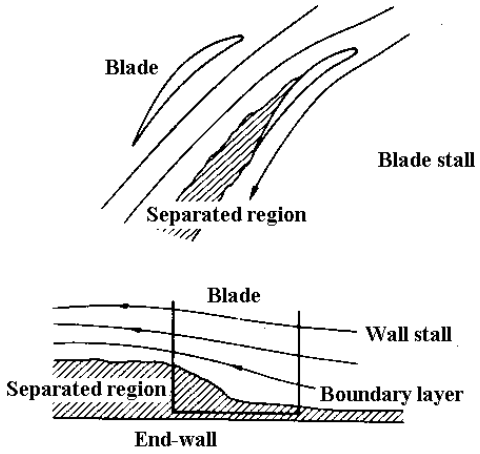

Fig. 1 Illustrating model of stall types, Greitzer et al. [2]

Hill et al. [5] carried out an experimental investigation into the influence of a vaned recess casing treatment on the performance of an industrial-type axial flow fan with a hub to tip ratio of 0.4. The treatment has been tested in a variety of configurations relative to the fan, with an emphasis on the amount of fan blade tip exposure to the treatment.

Bayomi, [6] and Rautenberg et al. [7] tested a radial flow compressor with a solid wall casing and with many different circumferentially grooved casings over the impeller leading edge. They showed that the groove geometry, (i.e. the depth, angle, number and spacing of the grooves), has a major effect on casing treatment.

Osborn et al. [8] and Moore et al. [9] reported that the casing treatment in axial compressors or fans improves the stall margin by displacing the stall (rotating stall) point to a lower weight flow region than that with a solid casing. Although, the basic mechanism of operation of the casing treatment is still not understood, the measurement that have been carried out show clearly that the treatment reduces the boundary layer blockage associated with the end-wall and retards the onset of rotating stall. Therefore, with a view of investigation of this mechanism, the objective is to conduct a series of experiments using a low speed flow tunnel (Mach number = 0.1).

CONCEPT OF PRESENT WORK

The experimental design process is completed by the choice of three variables, namely the width of the grooves, the depth of the grooves, and percentage open area (total area of grooves compared to total treatment area). As to width, there is evidence to suggest that the width should not exceed the blade thickness**,** Greitzer et al. [2]. Thus the width was chosen to be of the order of the blade thickness. The width of slot or groove has variously been tied to blade geometry, boundary layer geometry. Since, no signal methods appear to be advantageous, thus, the depth of treatment was arbitrarily chosen. As regards the percentage open area the treatments have taken to be between 12.5% and 25%, although this would appear to be matter of convenience, Macdougal and Elder, [10]. In particular, there is at present no fundamental theoretical understanding of the mechanism by which the grooves alter the behavior of the compressor. Such understanding would be useful in selecting and optimizing the treatment configuration. The present work, therefore, is a detailed attempt to develop a general qualitative framework to clarify the diversity of test results reported in the literature and to provide some guide as to the effectiveness of casing treatment grooves in a given situation. This is done through a series of experiments, which were designed specifically to vary the degree of influence of the treatment on separated boundary layer i.e. boundary layer subject to strong adverse pressure gradient as shown in Fig. (2). Therefore, a strong adverse pressure gradient boundary layer flow is going to be established in an open circuit wind tunnel and the groove will be introduced at point similar to point ITD in Fig. (2). The value of the shape factor at point D is equal to 2.8. Thus, recording the flow characteristics with and without the groove presence will give a fundamental understanding to the mechanism by which grooves alter the wall stall in compressors.

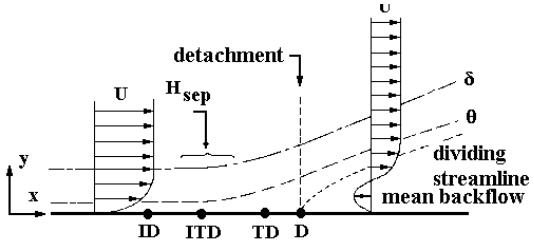

ID : incident detachment
ITD : intermittent transitory detachment
TD : transitory detachment
D : detachment

Fig. 2 Definitions of flow characteristics for two-dimensional separated boundary layer

EXPERIMENTAL PROCEDURE

An open circuit boundary layer wind tunnel of working section, 210 x 420 mm by 3.25 meters long, is used. More details are described by Higazy and Bayomi [11]. The freestream turbulence level is 2%, based on the streamwise velocity component, and the streamwise pressure gradient could be controlled by means of a flexible adjustable roof height. Boundary mean velocity profiles were measured on the working section floor using a digital micro-manometer and associated instrumentation, details of these facilities are given by

Higazy and Bayomi [12]. The velocity profiles were measured at various streamwise locations on the plate surface, giving an overall view of the entire flow field. A two–dimensional trip wire 1.2 mm in diameter was fixed to the plate surface 50 mm downstream from the leading edge. The diameter of the trip wire is chosen to satisfy the limiting condition reported by Schlichting [13]. The static pressures in the groove were measured referenced to the tunnel static pressure with a high precision calibrated digital micro-manometer Model Yokogawa 2655, with a measured range of -1000 mm of H_2O at an accuracy of $\pm$0.4%. As the pressure readings fluctuate with time, readings are recorded by a personal computer using an A/D converter and an average of readings is computed every 5 sec. Different configurations for tested grooves are shown in Fig. (3). The depth of groove, D is varied from 4 cm to 8 cm and the base length is varied from 4 to 12 cm. The width of the groove is constant and equal 42 cm. The ratios of the length to depth ratio are 1.0, 0.667 and 0.5.

ESTABLISHING OF SEPARATED BOUNDARY LAYER

Establishing of separated boundary layers on a smooth wall has criteria to be satisfied which is the shape factor to be equal to 2.8 as shown in Fig. (2). Thus, by analogy with laminar self-similar boundary layers an equilibrium turbulent boundary layer is one for which the gross properties of the inner region, constituting some 10-20% of the total boundary layer, can be scaled with a single parameter such as the boundary-layer dimensionless thickness Y^+, where $U^+ = (1/k)\ (\ln Y^+) + 5.1$, where k=0.41. In a turbulent boundary layer both logarithmic velocity-profiles and shear-stress profiles are self-similar. This self-similarity of logarithmic-velocity profiles implies, as Coles and Hirst [14] originally demonstrated that in a turbulent boundary layer U^+ is a function in Y^+ only. Hence is a similar U^+ unique function and thus in such a boundary layer the defect shape factor G, will be a constant. Through algebraic manipulation the conventional shape factor H, which is the rate of displacement thickness δ^* to momentum thickness θ, can be expressed in terms of the defect shape factor G given by $H = [1-c_f/2)^{0.5}\ G]$. This relationship shows that H is only constant in an equilibrium turbulent boundary layer if the local skin fraction c_f, is invariant with the distance *x* over which the boundary layer develops**.** Rotta [15] demonstrated that this latter condition is necessary if the whole boundary layer, including the logarithmic region, is to be in equilibrium.

However, special-purpose surfaces with appropriate roughness distributions are required to achieve it. In practice, therefore, in an equilibrium boundary layer the defect shape factor remains constant but, depending on the skin friction coefficient distribution variation, some streamwise variation of the shape factor H will occur.

Clauser [16] also showed that the condition to be satisfied for a turbulent boundary layer to be in equilibrium was the maintenance of a constant value of pressure-gradient parameter β along the developing layer. This parameter, equal to $(\delta^*/\tau_w)(dp/dx)$, determines the ratio of the pressure-imposed forces to the shear forces, which together cause the rate of change of momentum in the boundary layer. In practice it has been shown that constancy of β can be assured by maintaining the variation of free-stream velocity U with streamwise distance x in such a way as to satisfy U proportional to x^m, where for a given equilibrium layer m is a constant. Thus, incompressible two-dimensional turbulent boundary layer flows which are acceptably close to equilibrium can be obtained if the following conditions are satisfied: (i) the shape factor H either remains constant or decreases only very slowly as the momentum thickness-based Reynolds number R_θ increases; (ii) the momentum thickness of the boundary layer grows linearly with streamwise distance x; (iii) the free-stream velocity satisfies the relationship $U \propto x^{-m}$.

DETAILS OF BOUNDARY LAYER ESTABLISHED

The boundary-layer tunnel in which equilibrium flow of increasing pressure adversity was established and fully described as given by Higazy and Bayomi [12]. It has a uniform width of 420 mm and an inlet contraction of 10:1 area ratio. Equilibrium flow having different values of *m* can be established over the 3.2 m available for boundary-layer development by adjustment of a new designed flexible roof to the working section so that appropriate free-stream velocity distributions are developed. Downstream of the contraction the height of the working section is 228 mm, giving it a 2:1 aspect ratio at inlet.

CHARACTERISTICS OF THE FLOW ESTABLISHED WITHOUT GROOVE

The boundary layer integral parameter for clean surface is plotted against streamwise distance in Fig. (4). From this figure it can be seen that the momentum thickness increased linearly along the streamwise direction; while the shape factor and skin friction coefficient are almost constant along the streamwise direction.

The required two-dimensionality was verified by two methods as described by Higazy and Bayomi [12]. First by seeking to satisfy the equality between two sides of the integrated von Kármán momentum equation and second by determining the deviation in the wake flow resulting from two pin needles mounted at an upstream position on the wind tunnel floor. Satisfactory result was obtained over the 80% of the tunnel floor.

CHARACTERISTICS OF THE FLOW ESTABLISHED BEHIND GROOVE

The grooves were placed at a position on the floor where the shape factor H, was equal to 2.2 i.e. a turbulent boundary layer near separation. The university of the velocity profiles obtained with this boundary layer flow is in the logarithmic velocity graphs for clean surface and different types of grooves shown in Fig. (5).

A typical semi-logarithmic plot, Fig. (5), of the boundary layer development after the grooves shows the boundary layer-wake characteristics of the boundary layer. This structure change is accompanied by the groove geometry. The velocity profile of the boundary layer downstream of the groove carries an inflexion point. The upper limits of the application range of the logarithmic range of logarithmic law are Y^+=250 at station 5 and 300 at station 11.

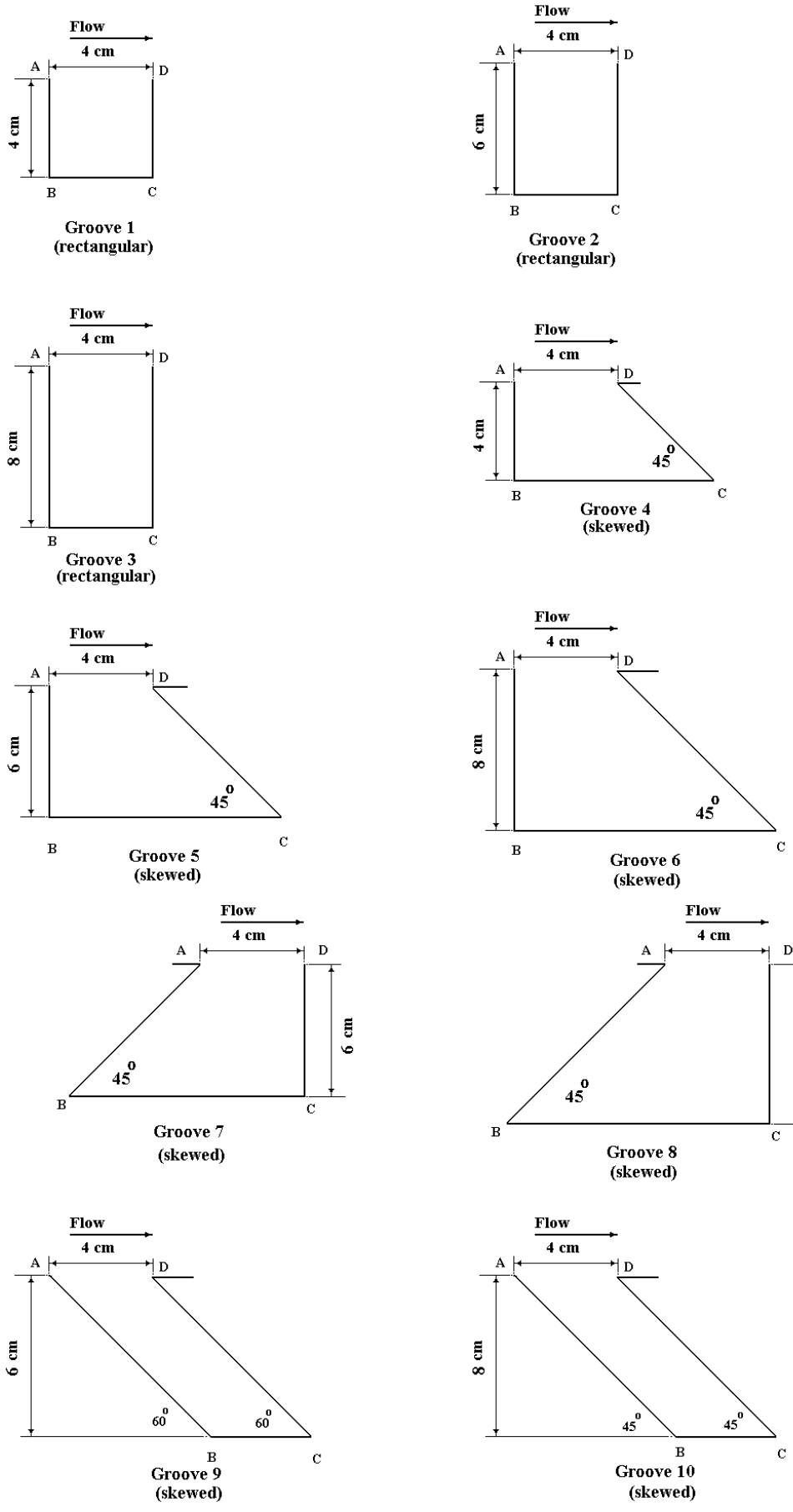

Fig. (3) Grooves geometry used in the present investigation.

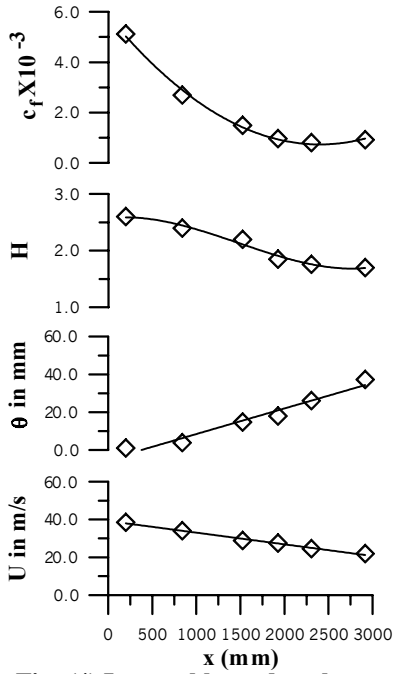

Fig. (4) Integral boundary layer paramter for clean surface.

Typical surface pressure distributions for ten grooves are presented in Fig. (6). The grooves tested here are of the open types as described by Higazy and Bayomi [11]. The major mechanisms dominate the surface pressure inside the groove, namely vortices in the groove, the boundary layer impingement and the recompression of the flow near the trailing edge of the groove. Spanwise vortex develop on the floor of the groove is also revealed by oil flow visualization. Similar flow visualization results are given by Higazy and Bayomi [11]. When the groove is deep i.e. l/D is less than one, the recompression of the flow and the momentum diffusion across the boundary layer become increasingly important. This results in a pressure rise on the floor of the groove well before the downstream corner of the groove. When the length to depth ratio of the groove decreases, the surface pressure along the upstream face of the groove gradually decreases due to the increased momentum diffusion of the boundary layer spanning the groove.

The momentum thickness, the skin friction coefficient and the shape factor behind the grooves are shown in Fig. (7). The shape factor distributions increase substantially after reattachment and then decrease again in the relaxation region. For example the value of the shape factor rises by about 33.3% for groove 3 and decreases again to about the value of the clean surface value. The form drag coefficients of the groove calculated from the pressure difference along the upstream and downstream faces of the groove are presented in Fig. (8). When the groove is rectangular, the drag coefficient rises with the length to depth ratio of the groove; since the momentum diffusion becomes weak in these flow mechanisms. In these grooves, the pressure on the upstream face of the groove drops due to the momentum diffusion across the boundary layer. Simultaneously, the pressure on the downstream face of the groove rises due to the recompression of the flow and a large downstream deflection of the boundary layer near the trailing edge of the groove. This brings the dividing streamline down towards the floor of the groove and subsequently causes an increased dynamic pressure towards the stagnation point. The combined effects are to increase the drag coefficient. When the groove is skewed, the momentum diffusion begins to play an important role in determining the mass and momentum balances of the groove flow. The onset of the boundary layer is expected to bring additional momentum into the groove, which would increase the drag of the groove as shown for skewed grooves in Fig. (8).

DISCUSSION AND CONCLUSION

The groove flows driven by separated boundary layer are reattached or relaxed flow. In the deep rectangular groove, the boundary layer is controlled by a transverse mechanism, while in the skewed groove, the separated boundary layer is controlled by a longitudinal mechanism.

There are different vortex structures associated with the transverse and longitudinal mechanism. The flow in a skewed groove in a longitudinal fashion is characterized by a large trailing edge vortex and vortices shed from the leading edge of the groove in an orderly manner. The movement of a single vortex in the groove characterizes the transverse mechanism. The transverse mechanism tends to be dominated by a low order mode when the length to depth ratio of the groove is deep i.e. $l/D \leq 0.5$. With the rise of the length to depth ratio of the groove, the dominant longitudinal mechanism mode increases. At $l/D=1$ the longitudinal mechanism occurs in a mode of higher order than that at $l/D<1$. With the onset of the longitudinal mechanism, the magnitude of the transfer rises sharply. After the transfer is established, the level of mechanism gradually decreases with increasing length to depth ratio of the groove due to the increased diffusion in the boundary layer. The longitudinal groove flow has a large influence downstream, The orderly vortical structures are generated by the vortices and the boundary layer spanning the groove. In a short groove, the pressure is characterized by the large vortex stationed near the trailing edge. With the rise of the length to depth ratio of the groove, diffusion in the boundary layer causes a pressure drop in the upstream half of the groove. In the mean time, the large downward boundary layer deflection causes a recompression near the trailing edge of the groove and subsequently a pressure rise in the downstream half of the groove. The onset of the longitudinal mechanism is expected to increase the form drag of the groove. The following remarks have been concluded:

1- The rectangular and skewed grooves flow driven by strong adverse pressure gradient are two types; transverse for rectangular grooves and longitudinal for skewed grooves.

2- The vortex structure for transverse rectangular flow in rectangular grooves is characterized by single vortex while the longitudinal skewed grooves flow have large vortex mixed with trailing edge vortex.

3- Skewed grooves were eliminating the high-pressure areas behind the grooves and thus, reducing the skin friction coefficient and the shape factor of the near separated boundary layers.

4- Pressure coefficients are influenced by the vortex and boundary layers spanning the groove. The skewed groove is distinguished by large vortex, while for rectangular grooves the transverse flow is identified by single vortex along the divided streamline over the groove.

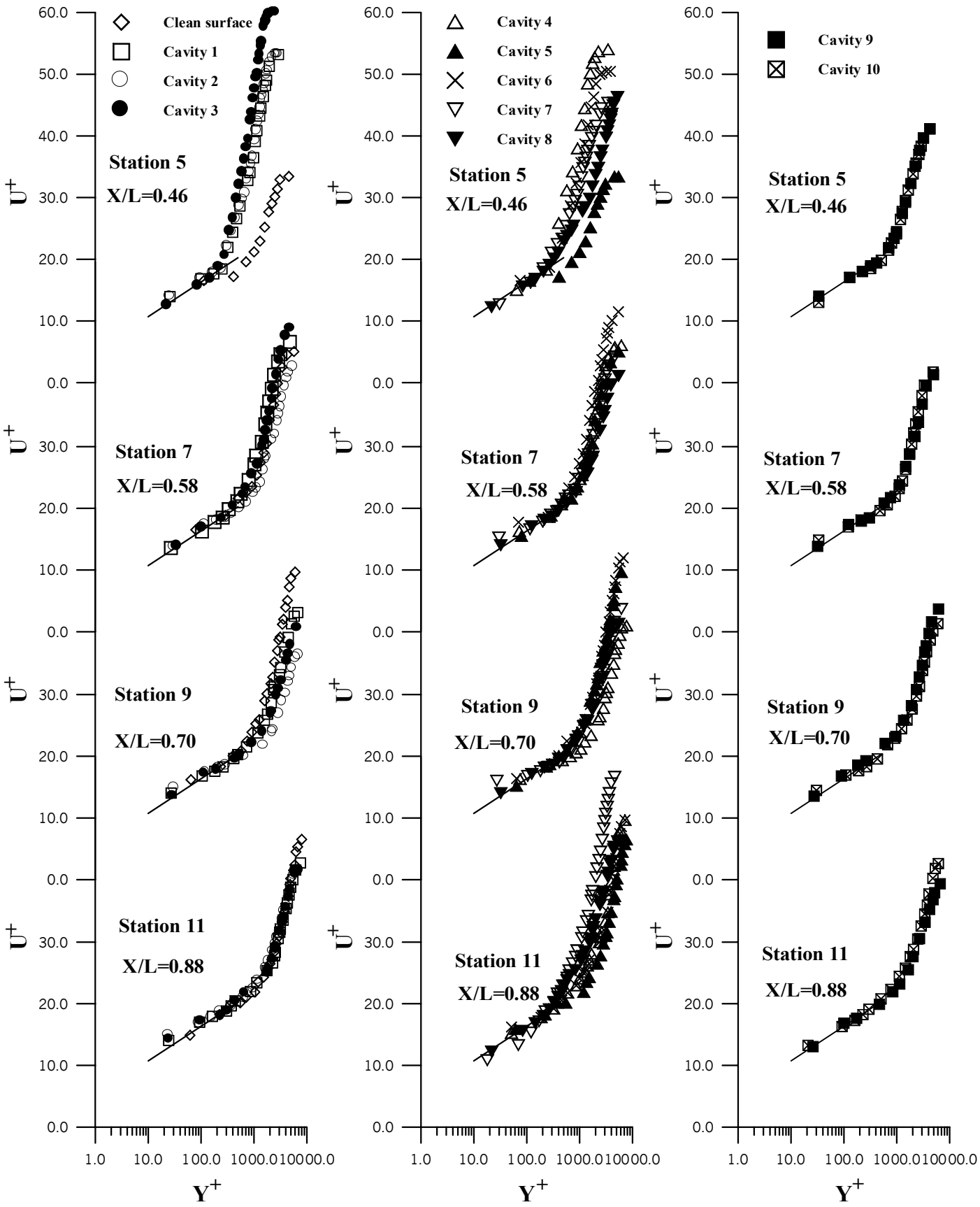

Fig. (5) Semi-Logarithmic plot of the boundary layer at various positions for clean surface and behined grooves. —— Eq. ($U^+=(1/0.41)\ln Y^+ +5.1$)

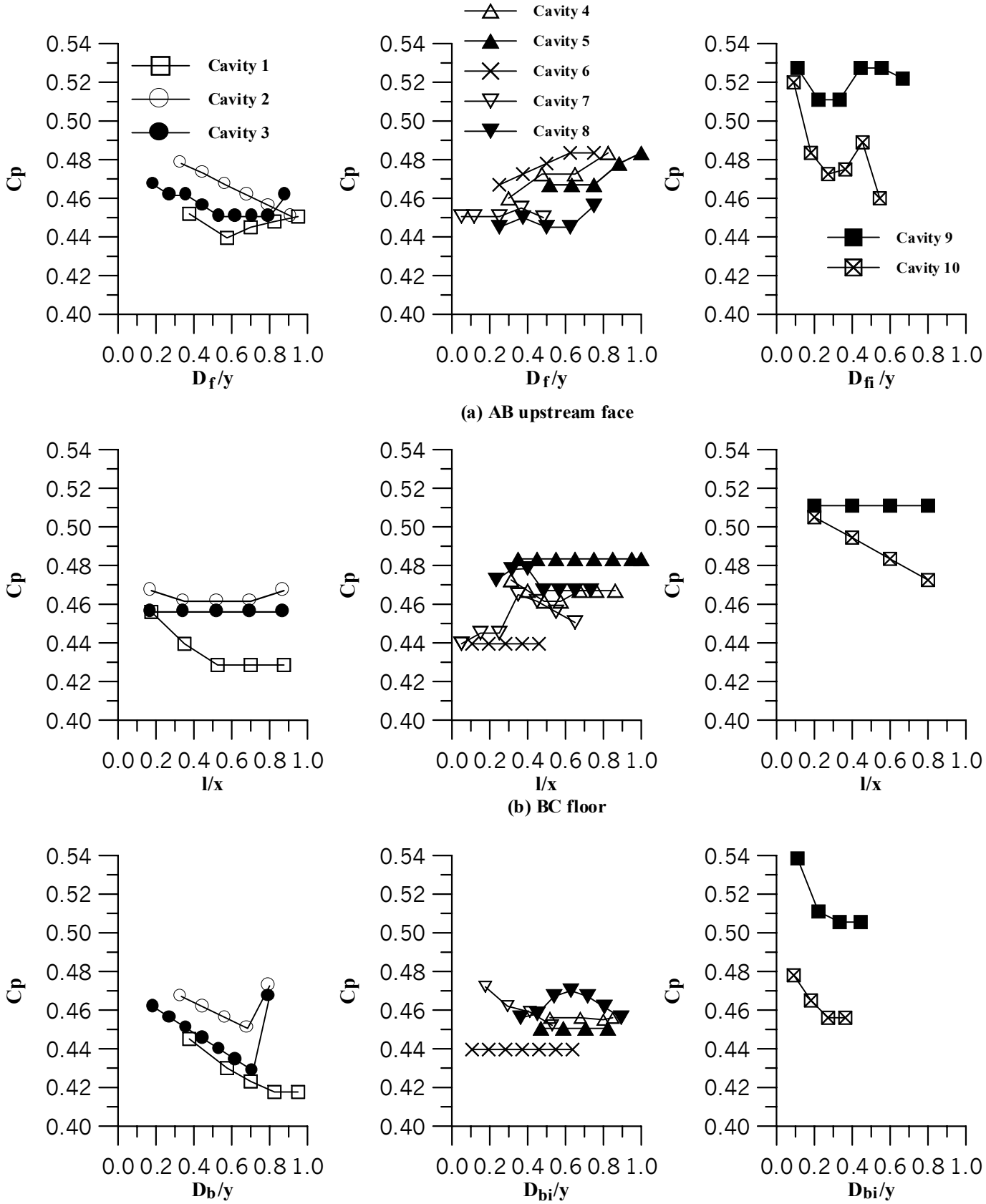

(a) AB upstream face

(b) BC floor

(c) CD downstream face

Fig. (6) Pressure surface coefficient distribution.

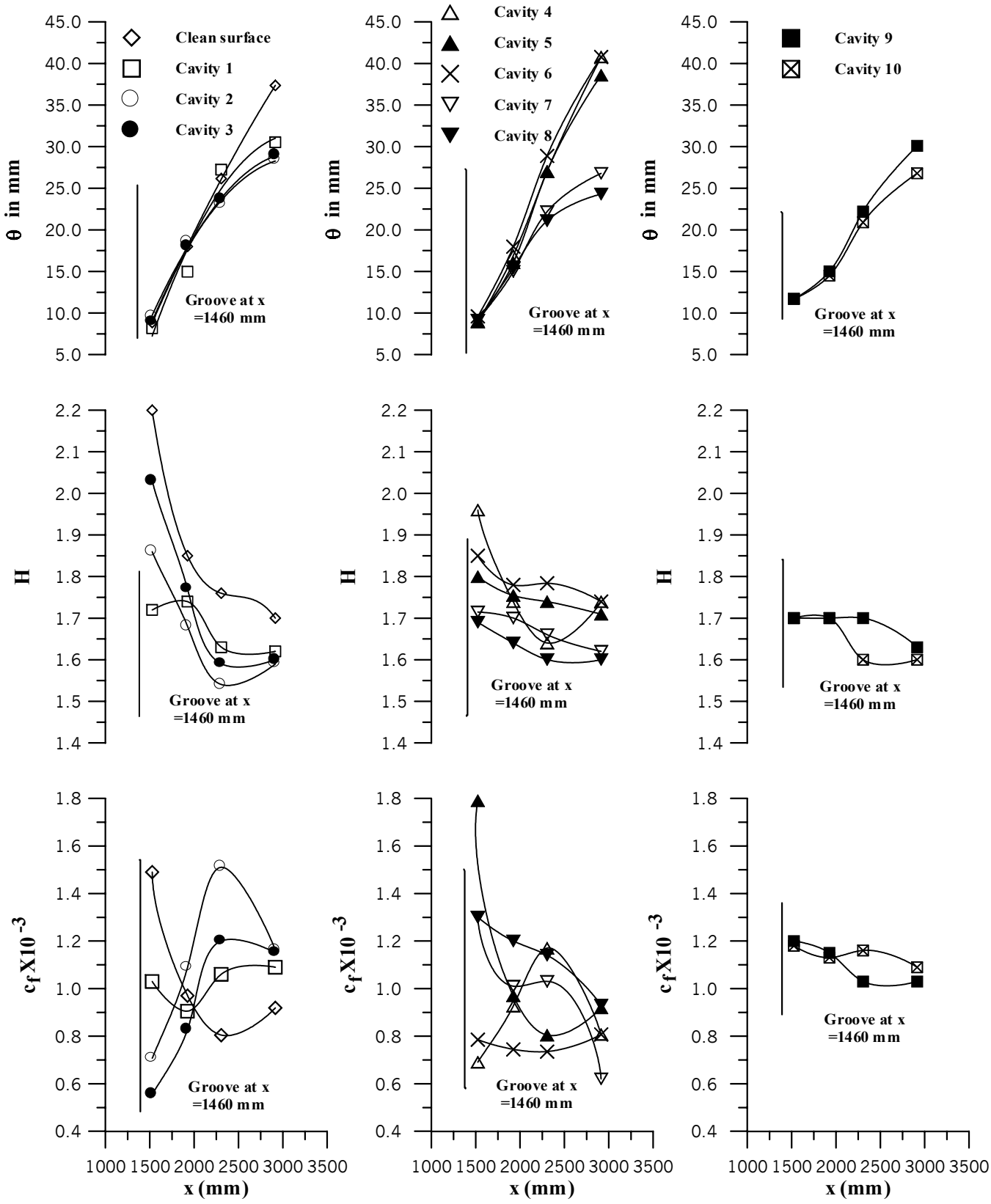

Fig. (7) Variation of boundary layer integral paramter behind grooves and for clean surface.

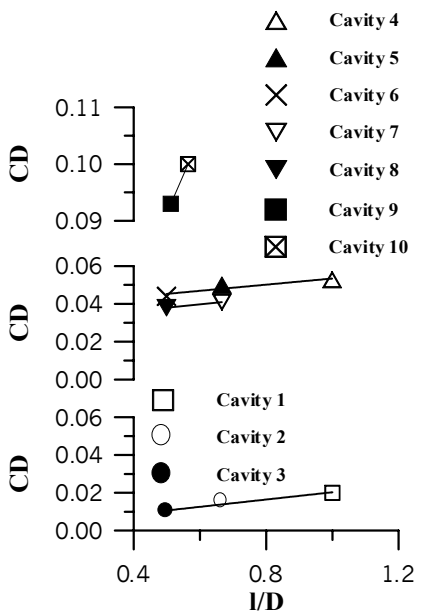

Fig. (8) Effect of groove configuration on the drag coefficient.

REFRENCES

1. Emmons, H. W., Pearson, C. E., and Grant, H. P., 1955, "Compressor surge and stall propagation," Trans. ASME, Vol. 77, No. 4, May, pp. 455-467.

2. Greitzer, E. M., Nikkanen, J. P., Haddad, D. E., Mazzawy, R. S., and Joslyn, H. D., 1979, "A fundamental criterion for the application of rotor casing treatment," Trans. ASME, J. of Fluids Engineering, Vol. 101, June, pp. 237-247.

3. Haupt, U., Rautenberg, M. and Abdel-Hamid, A., N., 1987, "Blade excitation by broadband pressure fluctuations in a centrifugal compressor," ASME paper 87-GT-17.

4. Johnson, M. C. and Greitzer, E. M., 1987, "Effects of slotted hub and casing treatments on compressor end-wall flow fields," Trans. ASME, J. of Turbomachinery, July, Vol. 109, pp. 380-387.

5. Hill, S. D., Elder, R. L. and McKenzie, A. B., 1998, "Application of casing treatment to an industrial axial-flow fan," Proc. Instn Mech. Engrs, Part A, Vol. 212, pp. 225-233.

6. Bayomi, N. N., 1995, "An investigation on the casing treatment of the radial compressors," Ph.D., Mataria, Helwan University, Cairo, Egypt.

7. Rautenberg, M., Heikal, H. A., Said, M. H. and Bayomi, N. N. 1998, "Investigation on increasing surge and stall margins of a centrifugal compressor using casing treatment," Engng. Res. Jour., Vol. 56, pp. 43-57, April, Helwan University, Faculty of Engng., Mataria, Cairo, EGYPT.

8. Osborn, W. M., Lewis, G. W., Jr., and Heidelberg, L. J., 1971, "Effect of several porous casing treatments on stall limit and on overall performance of an axial-flow compressor rotor," NASA TN D-6537.

9. Moore, R. D., Kovich, G. and Blade, R. J., 1971, "Effect of casing treatment on overall and blade-element performance of compressor rotor," NASA TN D-6538.

10. Macdougal, I., and Elder, R. L., 1982, "The improvement of operating range in a small high speed centrifugal compressor using casing treatments," IMechE, pp. 19-26.

11. Higazy, M. G. and Bayomi, N. N., 2000, "Experimental investigation of flow field characteristics over two cavities in tandem," 11th International Mechanical Power Engineering Conf. (IMPEC 11), Helwan University, Faculty of Engng., Mataria, 5-7 Feb., Cairo, EGYPT

12. Higazy, M. G. and Bayomi, N. N., 2000, "Assessment of two-dimensionality associated with drag of grooves measurement in turbulent boundary layers," Engng. Res. Jour., Vol. 71, pp. 133-147, October, Helwan University, Faculty of Engng., Mataria, EGYPT.

13. Schlichting, H., 1968, "Boundary layer theory," 6th Edition, McGraw Hill, New York.

14. Coles, D. E. and Hirst, E. A., 1968 "Proceedings computation of turbulent boundary layers," AFOSR-IFP, Stanford Conference, Vol. 2, pp. 47-54.

15. Rotta, J. C., 1962, "Turbulent boundary layers in incompressible flow," Prog. Aero. Sci., Vol. 2.

16. Clauser, F., 1954, "Turbulent boundary layers in adverse pressure gradients," J. Aero. Sci., 21.